NASA DEVELOP National Program
Virginia – Langley

Summer 2022

Delaware Basin Ecological Forecasting

Identifying Vegetation Trends and Atmospheric Stressors in the Guadalupe Mountains and Carlsbad Caverns National Parks

DEVELOP Technical Report
Final– August 11th, 2022

Jack Mezger (Project Lead)
Mark Bossinger
Gillian McNamara
Quinn Heiser

Advisors:
Joseph Spruce (Science, Systems, and Applications, Inc.)
Dr. Kenton Ross (NASA Langley Research Center)
Dr. Elizabeth Wiggins (NASA Langley Research Center)

Previous Contributors:
Sean Cusick
Amber Schlessiger
Billy Henshaw
Perrin Krisko

1. Abstract

The Guadalupe Mountains and Carlsbad Caverns National Parks, located in the Delaware Basin in the southwestern United States, experienced both a decrease in precipitation and an increase in temperature over the last decade. Furthermore, activity from local oil fields generated nitrogen dioxide (NO_2) plumes that spread over the parks could also have negative impacts on vegetations. NO_2 is a precursor for tropospheric ozone (O_3) which is known to have adverse effects on vegetation and ecosystems at large. These new climate dynamics prompted the National Park Service (NPS) to collaborate with NASA DEVELOP to assess the impact on vegetation within the parks from various stress factors. We used NASA Earth observations including Landsat 5 Thematic Mapper (TM), Landsat 7 Enhanced Thematic Mapper (ETM+), Landsat 8 Operational Land Imager (OLI), and Global Precipitation Measurement Integrated Multi-Satellite Retrievals (GPM IMERG) to assess vegetation health, water stress, and precipitation in the affected parks. After creating a homogenous reference area in the Sierra Diablo Mountains, the team visualized vegetation health through a Normalized Difference Vegetation Index (NDVI) time series map from 2010-2021. Our analyses did not show strong evidence that the NO_2 plume is causing vegetation decline. At the same time, this does not necessarily mean the effect is small because our method did not account for other factors that affect vegetation health. Following this, we created a water stress map with a Normalized Difference Moisture Index (NDMI) time series map from 2010-2021, which revealed a pattern of increasing water stress. We also confirmed that precipitation in the region decreased over the span of 2010-2021. These observations and findings will allow the NPS Intermountain Region to more effectively plan for the preservation and maintenance of vegetation health within the parks.

Key Terms

Ecological Forecasting, Remote Sensing, Vegetation Monitoring, NO_2 Impact, Drought

2. Introduction

2.1 Background Information

Located within the Delaware Basin, Carlsbad Caverns National Park (CAVE) and Guadalupe Mountains National Park (GUMO) run along the Texas and southern New Mexico border (Figure 1). The basin is a part of the greater Permian Basin, which is known for its vast quantities of oil and gas. According to the U.S. Energy Information Administration (US EIA, 2022), the Permian Basin produces upwards of five million barrels of oil and more than twenty trillion cubic feet of natural gas per day. Other than 2020, the first year of the COVID-19 pandemic, these figures have only increased over time. This is attributed to the introduction of fracking to the area in 2012 (Xiong et al., 2018). The use of diesel-powered equipment during and in preparation for the fracking process releases large amounts of air pollutants such as carbon dioxide (CO_2), sulfur dioxide (SO_2), particulate matter, and nitrogen dioxide (NO_2) (Jackson et al., 2014). Additional sources of pollutants during this process include natural gas leaks, intentional venting of oil and storage tanks, and flaring--the intentional burning of gases (Jackson et al., 2014).

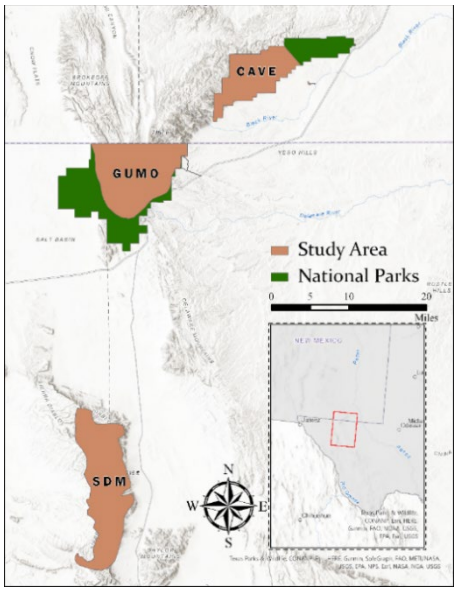

Figure 1. The boundaries of various areas within our study region are shown. CAVE and GUMO represent the study areas in the national parks while SDM represents the San Diablo Mountains reference area outside of the nitrogen plume.

Previous DEVELOP work conducted in partnership with the National Park Service (NPS) Intermountain Region found evidence for presence of NO_2 plumes, originating east, over both CAVE and GUMO (Cusick et al., 2022). NO_2 adversely affects vegetation health by reducing photosynthetic activity and precipitating acid rain (Gheorghe & Ion, 2011). Acid rain in turn can alter soil pH, inducing aluminum cation (Al^{3+}) toxicity in vegetation as a result (Gheorghe & Ion, 2011). Except for needles in conifer species, such conditions render younger plants and plant tissue the vulnerable to negative effects (Gheorghe & Ion, 2011). Visible symptoms of deterioration due to NO_2 are most seen as chlorosis (yellowing) of leaves and tip burn of needles (Gheorghe & Ion, 2011). NO_2 is also a known precursor to tropospheric ozone (O_3), another stressor that impacts many aspects of natural ecosystems (Grulke & Heath, 2019). Often provoking some of the same visual plant injuries as NO_2, O_3 damages vegetation through a similar mechanism to NO_2: entering the leaf via normal gas exchange and worsening cell integrity (Krupa & Manning, 1988). On a broader scale, studies have shown that O_3 stunts the growth of mature trees in some locations; if there are decades of exposure, O_3 may alter the species composition of the ecosystem entirely (Grulke & Heath, 2019).

During our study period of May 2010 – May 2021, a mega-drought impacted the southwestern United States with increasing severity (Apurv & Cai, 2021). Drought conditions have degraded vegetation across the region in part through depletion of soil moisture and groundwater (Apurv & Cai, 2021). CAVE and GUMO have observed these conditions within the parks in the form of increasing temperatures and decreasing precipitation in recent decades. Previous studies have utilized remote sensing techniques to accurately measure vegetation health in response to a variety of stressors. Qu et al. (2019) found that the Vegetation Health Index calculated from NASA's Moderate Resolution Imaging Spectroradiometer (MODIS) correlated highly with rainfall anomalies in an area experiencing extreme drought. Another study evaluating remote sensing to track vegetation stress suggests that such methods can identify ozone-induced plant stress before visible effects are present (Meroni et al., 2009). Using similar techniques, this project quantified both general vegetation health as well as water stress in CAVE and GUMO in order to isolate the effects of NO_2 plumes on vegetation.

To facilitate this, we defined study areas within the greater park boundaries of CAVE and GUMO. This region of Texas and New Mexico is a semi-arid environment, so a considerable amount of CAVE and GUMO is sparsely vegetated or has no vegetation at all. Because our project focused on the impacts on vegetation, we created subsets of more densely vegetated areas in CAVE and GUMO that would serve as our study areas for both parks. In addition to this, we needed a reference area to act as a control that was outside of the NO_2 plumes. We chose the Sierra Diablo Mountains (SDM) due to the elevation, precipitation trends, and vegetation types being comparable to CAVE and GUMO.

2.2 Project Partners & Objectives

The NPS Intermountain Region, Carlsbad Caverns National Park, and Guadalupe Mountains National Park served as the project partners. The NPS has observed a reduction in air quality over CAVE and GUMO over the last decade. Partners are concerned about the adverse effects on vegetation health from deteriorating air quality, and how to separate them from the effects from observed decreases in precipitation and increases in temperature due to drought. Staff at CAVE and GUMO evaluate their respective parks' health to inform decisions relating to oil and gas leases made by the Bureau of Land Management and state agencies. The NPS Intermountain Region protects ecosystem functions and facilitates positive visitor experiences through understanding threats to vegetation health and resources. By expanding on past DEVELOP partnership work, the NPS Intermountain Region aims to gain knowledge of vegetation health status in the parks that can aid in making management decisions.

The project objectives consisted of the following: first and foremost, to identify changes in vegetation health within the national parks from May 2010 to May 2021 by creating a vegetation health map. The second objective was to quantify drought effects on vegetation by creating both a vegetation water stress map and a precipitation time series over the same period. The third and final objective was to compare these trends with the observed NO_2 plumes over the Delaware Basin in order to isolate drought-induced vegetation health changes from changes generated by the NO_2 plumes.

3. Methodology

3.1 Data Acquisition

This study's timeframe encompassed May 2010 – May 2021 and because of this, we used data from NASA's Landsat 5 Thematic Mapper (TM), Landsat 7 Enhanced Thematic Mapper (ETM+) and Landsat 8 Operational Land Imager (OLI) (U.S. Geological Survey, 2020). Landsat 8 was not in orbit until April 2013; therefore, we used Landsat 5 and Landsat 7 to monitor vegetation health and water stress from January 2010 to January 2013. Landsat 5 was used from January 2010 – January 2012 in place of Landsat 7 due to the failure of the scan line corrector aboard Landsat 7 in 2003 (Markham et al., 2004). Landsat 7 was used from January 2012 – January 2013 due to the gap between the decommissioning of Landsat 5 in June 2012 and the launching of Landsat 8 in April 2013. Each Landsat sensor used has a spatial resolution of 30m x 30m, comparable spectral bands, and nearly synonymous orbital paths. This makes the data compatible and adequate for use in this study (Table A1).

We acquired all Landsat imagery through the USGS EarthExplorer data portal. CAVE and GUMO are very close in proximity, permitting the use of only one scene throughout the project. We reduced the data parameters to the date range of interest, cloud cover of 0% - 5%, orbital path 32 row 38, and level two products. Because the project examined satellite data for more than a decade, we collected imagery on a quarterly basis. The months of December-February, March-May, June-August, and September-November represented the seasons of winter, spring, summer, and autumn, respectively. We collected one Landsat image within each of these time frames to represent its season.

With respect to precipitation data, we used NASA's Global Precipitation Measurement (GPM) mission, which includes the Integrated Multi-satellitE Retrievals for GPM (IMERG). Especially in comparison to the Tropical Rainfall Measurement Mission (TRMM), Multisatellite Precipitation Analysis 3B42 and the European Centre for Medium-Range Weather Forecast's ERA-Interim datasets, IMERG boasted higher temporal and

spatial resolutions, correlation to rain-gauge data, adjustment for daily timescale bias in comparison to ground data, detection of precipitation events such as Probability of Detection (POD), Critical Success Index (CSI), and False Alarm Ratio (FAR), and measurement results of precipitation under 15mm/day (Sharifi et al., 2016). IMERG data were acquired through NASA's Earthdata program between 2010 and 2021 in monthly intervals (Huffman et al., 2019). Individual bounding boxes were used to subset data for CAVE (32°3'N 104°39'W, 32°12'N 104°24'W), GUMO (31°48'N 105°W, 32°N 104°45'W), and SDM (31°9'N 105°W, 31°30'N 104°51'W).

Only 5 miles away from each other, CAVE and GUMO cover the same mountain range and thus share similar qualities. Elevation starts around 800 meters in the eastern portion of CAVE and steadily increases, moving southwest, to 2,600 meters at Guadalupe Peak. According to the U.S. Department of Agriculture's (USDA) LANDFIRE Vegetation Dataset, vegetation is comparable between the two areas. Woodland thrives in the higher elevations of this mountain range, with Madrean Pinyon-Juniper Woodland comprising the majority of land cover classes. Apacherian-Chihuahuan Semi-Desert Shrub-Steppe makes up the slopes of the mountains and Chihuahuan Mixed Desert and Thornscrub comprise the flatter, lower elevations. Through close visual analysis, park boundaries were clipped to highlight areas of Pinyon-Juniper. Apacherian-Chihuahuan Semi-Desert Shrub-Steppe were included, however much of the Chihuahuan Mixed Desert and Thornscrub were excluded. These news subsets allowed us to focus on woodlands for more accurate vegetation analysis. Additionally, these new subsets maintained similar elevation

To ensure a robust analysis, we needed to select a third area as a point of reference. Because of the short distance between the parks, differing effects of the westerly NO_2 plumes would be difficult to discern between the two study areas. We selected the SDM as the best point of reference based on its elevation, vegetation, location, and precipitation trends (Figure 1). The selected reference area's elevation does not exceed the maximum of GUMO or the minimum of CAVE. Woodlands in SDM are comprised of Madrean Pinyon-Juniper Woodland with similar vegetation types in the mid to lower elevations. Most important of all, SDM is located around 30 miles southwest of both parks and the eastern NO_2 plumes (Figure D1).

3.2 Data Processing

We began data processing by addressing the spatial data gaps in the Landsat 7 imagery. We interpolated the missing values using an inverse distance weighted approach through Geospatial Data Acquisition Library's (GDAL's) 'fillnodata' utility. Our processing incorporated a search radius of 10 pixels, which resulted in extremely low variation between interpolated and non-interpolated versions. Regarding the void interpolated areas, the mean and standard deviation did not vary more than 0.001 for Normalized Difference Vegetation Index (NDVI) or Normalized Difference Moisture Index (NDMI) values.

To evaluate vegetation health, we calculated the NDVI for each season of each year in QGIS as the inverse ratio of the near-infrared and red bands (Table B2). To account for drought effects on vegetation health, we also used QGIS to calculate NDMI as a ratio of the near-infrared and shortwave infrared bands for the entire dataset (Table B2). NDVI and NDMI derived from Landsat 5 and Landsat 7 are comparable and therefore did not need to undergo any transformation (Vogelmann et al., 2001), but NDVI and NDMI derived from Landsat 5 and Landsat 7 required a transformation to be comparable to Landsat 8 NDVI and NDMI due to differences in band designations by wavelength. We used a regression-based transformation to homogenize the values derived from Landsat 5 and 7 to Landsat 8. Additionally, we transformed the near-infrared (NIR) and shortwave infrared (SWIR) bands of the same satellites to create similar NDMI values (Table B2). In doing so, values become comparable across the entirety of the study period (Roy et al., 2016). We then clipped the resulting data for both indices to our study areas and reference area and into individual files. Lastly, the precipitation data were exported as Microsoft Excel files to be viewed as the processed monthly precipitation values as well as visualized in line graph form.

In order to detect trends in vegetation health and water stress, we created percent change maps for NDVI and NDMI in an interannual stepwise process, starting from spring 2010 and ending with spring 2021 (Table

B2). We also created change maps of the same indices using spring 2010 and spring 2021 to represent the overarching change over our entire study period in one image. The spring images had the most canopy cover of all the seasons, so we focused our change detection solely on spring to best observe decreases or increases in vegetation health and water content. The spring images also had the least cloud cover at <0.1% because the images were taken before the monsoon season, which typically begins in July. The spring images also showed a strong presence of NO_2 plumes, making them the most fit for analysis.

3.3 Data Analysis

For this analysis, we used change detection data from spring 2010 through spring 2021 to visualize change over the entire study period. NDVI and NDMI have been shown to have a strong linear relationship (Karan et al., 2016). To verify that the semi-arid landscape demonstrates a similar relationship between these indices, we conducted a regression analysis of all average NDVI and NDMI values collected. The two variables conjoined for a moderately strong r^2 of 0.565. Additionally, through an ANOVA statistical test, we produced an F-stat valued at 118.17 with a significance of <0.001 (Table B1).

We first analyzed the data through the creation of a bivariate choropleth map. We created this map to compare NDVI values to NDMI values found in the study areas and reference area. Considering this, we wanted to highlight inconsistencies in the data where, for example, NDMI had a large percent increase and NDVI had a large percent decrease or vice versa. Assuming that NDMI and presence of NO_2 are the only two factors affecting changes in NDVI, then areas in the choropleth map that are inconsistent with premise that NDVI and NDMI have a positive linear relationship should coincide with the presence of NO_2 plumes. We determined that either a ±25% change in NDVI or a ±50% change in NDMI over the study period was significant and set our classification thresholds as such (Table 1). We created this map by using conditional statements in ArcGIS Pro using one change detection map between spring 2010 and spring 2021. These conditional statements created 6 raster datasets for each study area NDMI (high, medium, low) and NDVI (high, medium, low). These raster datasets were designed so that 1 = true and 0 = false for each conditional statement. From this point, we used the raster calculator to calculate the class number associated for each specific raster. For example, to derive class 9 (Table 1), we used the raster calculator to multiply where NDVI is greater than 25% with where NDMI is less than 50%. This resulted in any value that is true for both becoming 1 while all others become 0. To set the value of this class to 9, we simply multiplied the resulting value by 9; the example equation for class 9 is as follows: (High NDVI) * (Low NDMI) * 9. We repeated this process for all 9 classes. Where NDVI is high, NDMI is expected to also be high due to the moderately strong linear relationship between the two indices. This resulted in classes 1 and 9 being strongly inconsistent (Table 1). Similarly, we determined classes 3, 5, and 7 to be consistent values as they aligned with this expected relationship (Table 1). "Moderately" was defined as less than a 25% difference in NDVI because that was within one standard deviation. "Significantly" was defined as more than a 25% difference in NDVI, but a 50% difference in NDMI. 50% difference in NDMI was not exactly one standard deviation but was found to be the best benchmark after trial and error.

Table 1

Classification of the bivariate choropleth map. This table displays the relationship between decay, stability, and growth to see if the linear correlation between NDMI and NDVI holds in the observed findings. For example, an increase in NDMI and a decrease in NDVI is classified as "inconsistent decay" because vegetation health is decreasing despite a higher presence of moisture.

Percent Change from Spring 2010 – 2021	NDVI < -25% (Low)	-25% < NDVI < 25% (Medium)	NDVI > 25% (High)
NDMI > 50% (High)	1 - Strongly Inconsistent Decay	2 - Moderately Inconsistent Decay	3 - Consistent Growth

-50% < NDMI < 50% (Medium)	4 - Slightly Inconsistent Decay	5 - Consistent Stability	6 - Slightly Inconsistent Growth
NDMI < -50% (Low)	7 - Consistent Decay	8 - Moderately Inconsistent Growth	9 - Strongly Inconsistent Growth

We also created multiple graphic interchange formats (GIFs) through ArcGIS Pro Animations to show side by side comparisons of CAVE, GUMO, and SDM. These GIFs display NDVI and NDMI change detection maps created annually between each spring over the entire study period. For example, the first image shown would be spring 2010 – spring 2011, the next would be spring 2010 – spring 2012, and so on. This allowed us to compare the alterations of NDVI and NDMI between the study areas throughout the study period and find areas in CAVE and GUMO that exhibit trends that cannot be explained by the effects of drought alone, and therefore could have been adversely impacted by NO_2 plumes.

To further analyze the GIFs, we viewed precipitation time series data alongside the NDVI and NDMI change detection maps year to year. The monsoon season for CAVE and GUMO usually starts in July. However, the monsoon season begins earlier than July in some years, which can cause an increase in NDVI and NDMI in the change detection maps. Therefore, it was important for us to be able to document this as a confounding variable and accurately measure the impact that it could be having on the data.

We were concerned with certain vegetation types being affected differently by air pollution or drought. To mitigate this, we used the LANDFIRE vegetation dataset to differentiate between vegetation that was classified as conifer, conifer-hardwood, grassland, shrubland, and riparian. Conifers and conifer-hardwoods consisted mostly of multiple types of Pinyon-Juniper Woodlands. Grasslands were mostly Apacherian-Chihuahuan. Shrublands were predominantly Thornscrub and Shrub-Steppe. The riparian class is representative of less than 2 percent of the areas. Therefore, the trends it exhibits are most likely not representative of the overall NDMI and NDVI trends in the region. We then examined the mean percent change for NDVI and NDMI between 2010-2021. We did this for all three areas: SDM, GUMO, and CAVE (Figure 2).

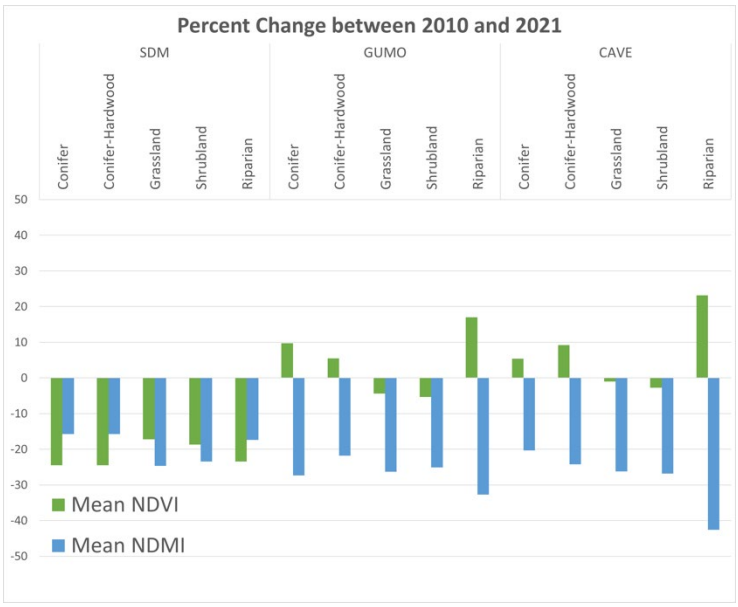

Figure 2. The average NDVI and NDMI changes between 2010 and 2021 are displayed. Each study area is represented by a conifer, conifer-hardwood, grassland, shrubland, and riparian vegetation class.

We also used data from the Spring 2022 Delaware Basin Health & Air Quality project in order to map the spatial distribution of the NO_2 plume. Comparing the previous term's NO_2 maps with our change detection maps allowed us to analyze vegetation that was directly under the influence of the NO_2 plume. With this information, we compared vegetation health inside of the plumes to vegetation health outside of the plumes to see if there was a stark contrast that could be attributed to the effects of NO_2 pollution.

4. Results & Discussion

4.1 Analysis of Results

4.1.1 Observed Trends

In comparing the mean NDVI values of each study area annually and including each season, the highest and lowest values for CAVE and GUMO are very similar. CAVE and GUMO have ranges of 0.106 to 0.178 (0.072 difference) and 0.101 to 0.171 (0.070 difference), respectively. The ranges for NDMI means of the two parks are almost as close, with a range of –0.067 to –0.008 (0.059 difference) for GUMO and a range of –0.078 to –0.014 (0.064 difference) for CAVE. The highest seasonal mean NDVI for both parks occurred in spring and summer of 2014. NDVI values in both areas for winter 2017 and winter 2021 were very low relative to the rest of the study period. CAVE's lowest mean NDVI (0.101) was found in winter 2021, coming close to its mean NDVI for winter 2017 of 0.108. GUMO's lowest mean NDVI (0.106) was found in winter 2017, coming close to its mean NDVI for winter 2021 of 0.112. This suggests that the two parks are similarly impacted by any changing environmental conditions in the region, such as drought. The SDM mean NDVI and NDMI values are relatively close to those of CAVE and GUMO, though they display tighter ranges; NDVI ranges from 0.094 to 0.148 (0.054 difference) and NDMI ranges from –0.078 to –0.034 (0.044 difference). The slightly reduced variation in both indices in SDM is an indicator of SDM's efficacy as a reference area.

CAVE and GUMO showed very similar changes based on class from 2010 to 2021; riparian, conifer, and conifer-hard increased in NDVI while shrubland and grassland decreased (Figure 2). Unlike the parks, SDM displayed consistent values across all vegetation classifications, with NDVIs decreasing by more than 10 percent. However, shrubland and grassland classes of SDM decreased the least within the study area, while

conifers and conifer-hardwoods lost the most NDVI. Trends of NDMI values did not change by classification, which is likely attributed to the mega drought of the area.

Once cross referenced with a Digital Elevation Model (DEM), we found the areas with higher elevation to show lower NDMI values (U.S. Geological Survey, 2015). Because the region is mountainous, water runoff is likely being concentrated in the same locations. Moreover, areas of runoff could likely represent a pooling of water runoff that could affect NDMI values. Both CAVE and GUMO had numerous canyons that could serve as locations for water runoff, while SDM's slope is not nearly as drastic. While there is spatial variation seen in the NDMI change detection maps, the overall trend is that NDMI is decreasing across the study areas therefore water stress is increasing (Figure 3).

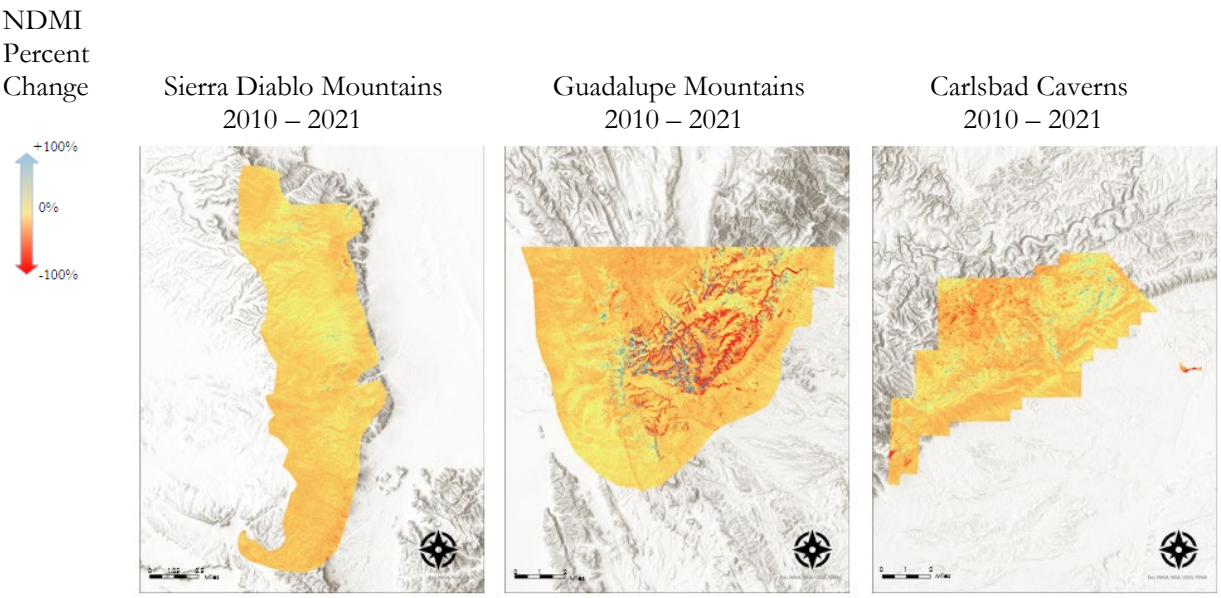

Figure 3. These maps display the NDMI percent change (change in water stress) between 2010-2021 in SDM, GUMO, and CAVE

We repeated the same process of cross-referencing the DEM for the NDVI change detection maps (Figure 4). We found that higher elevations contain most of the conifer and conifer-hardwood classes. In CAVE and GUMO, NDVI increased slightly in higher elevation climates. In contrast, lower elevations containing mostly shrubland and grassland classes experienced a decrease in NDVI. This spatial variability is more pronounced in CAVE and GUMO in comparison to SDM (Figure 4).

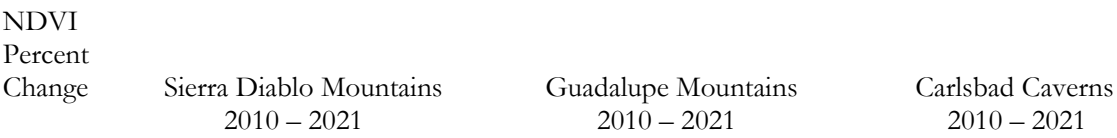

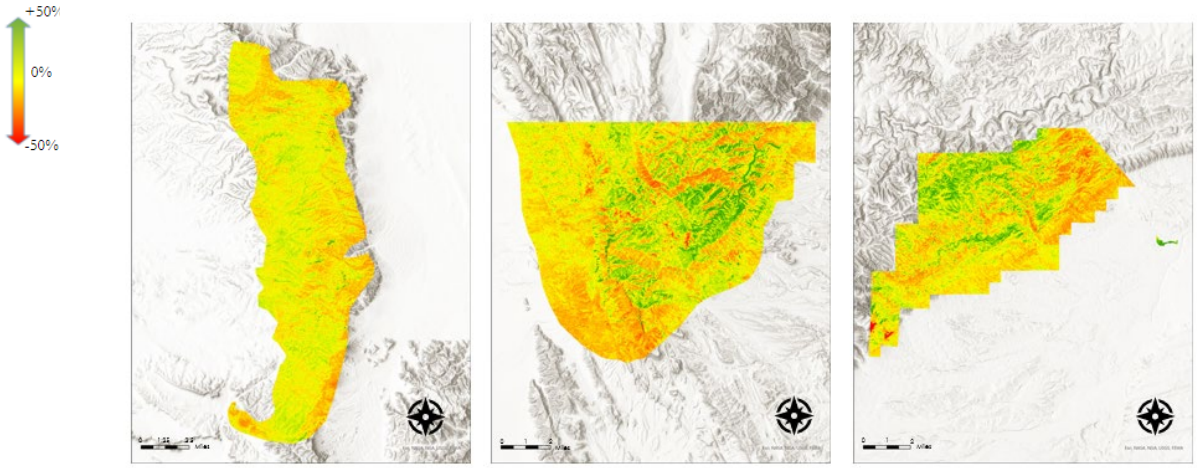

Figure 4. These maps display the NDVI percent change (demonstrating change in vegetation health) between 2010-2021 in SDM, GUMO, and CAVE.

Similar precipitation maximums and minimums were observed on an annual basis between the study areas. The monthly mean precipitation decreased over the course of the study period. The only exception to this is in 2011 – 2012 where there was a larger decrease due to severe drought in the region which was followed by a subsequent increase back to relatively average values in 2013 – 2014. While precipitation trends highlight periods of severe drought and lack of water availability, the precipitation trends are also similar enough between the study areas of CAVE and GUMO and the reference area of SDM that we determined precipitation would not be a confounding variable when comparing these areas for our study (Figure 5).

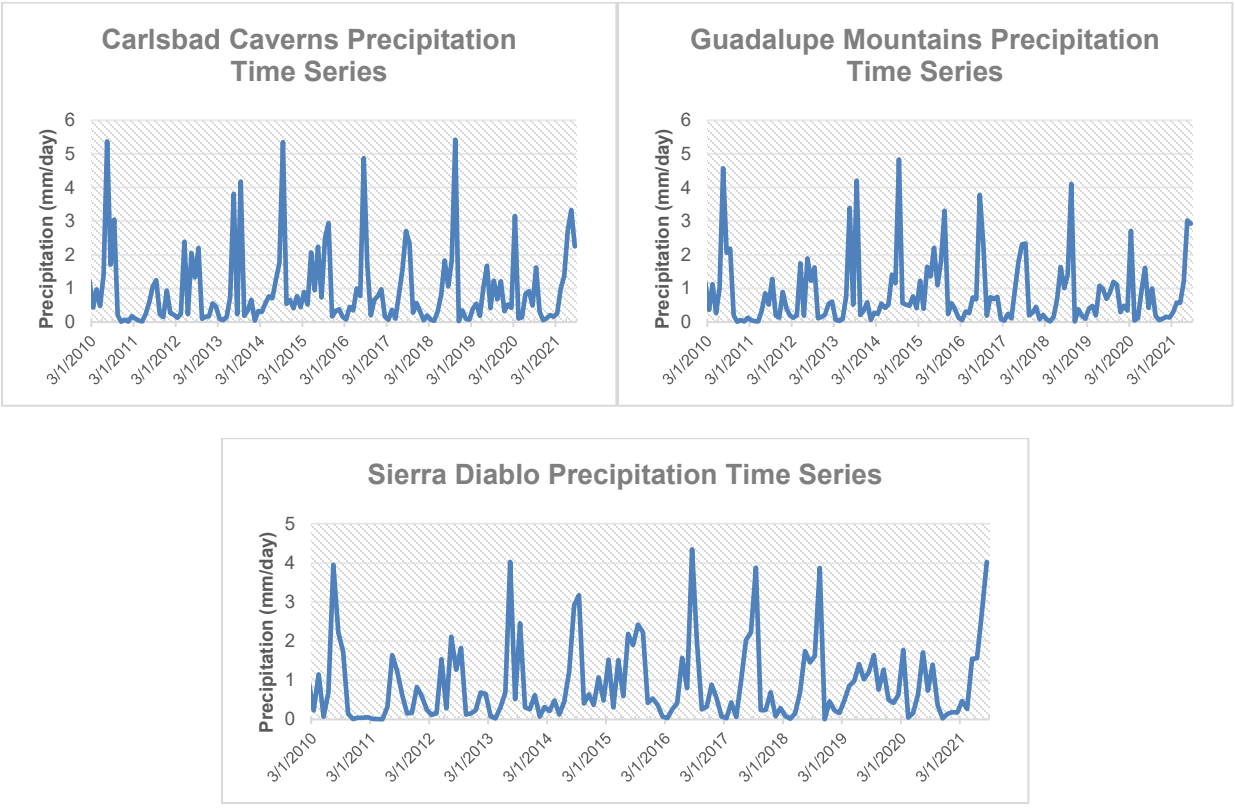

Figure 5. The precipitation data by month is displayed from 2010-2021 by study area.

4.1.2 Bivariate Choropleth

Based on the results of the changes in NDVI and NDMI, and using the classes from Table 1, the team created a 3x3 9-class bivariate choropleth map (Figure 6). This map allowed quantification of the proportion of inconsistent measurements over CAVE and GUMO which could be attributed to the effects of NO_2 pollution when referenced to SDM. We derived this by taking the sum of pixels in classes 3, 5, and 7 (the expected values) and dividing that number by the sum of total pixels. SDM had 98.5% of its pixels classified as consistent values, GUMO had 80.7% of its pixels classified as consistent values, and CAVE had 86.7% of its pixels classified as consistent values.

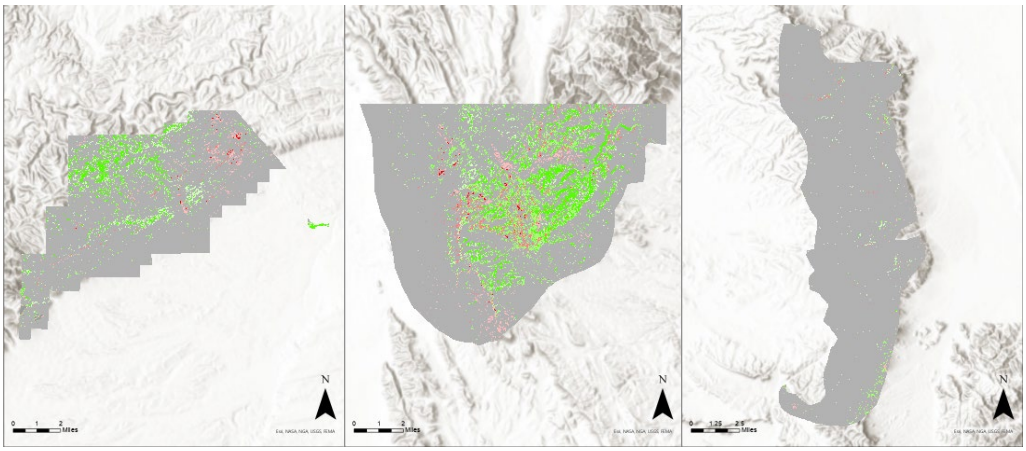

Figure 6. These are the bivariant choropleth maps generated through the classification outlined in Table 1. The colors correspond with the classes indicated in Table 1. CAVE, GUMO, and SDM are shown from left to right.

4.1.2 Errors and Uncertainties

The main goal with this project was to identify if NO_2 pollution was adversely affecting plants within CAVE and GUMO. Unfortunately, there were many confounding factors that could not be fully accounted for in the scope of this project. These factors include the megadrought in the American Southwest, the deriving of NDMI and NDVI values, the methods of retrieving Landsat data, wildfires, and nitrogen deposition.

The main confounding variable was the megadrought affecting the American Southwest (Apurv & Cai, 2021). Separating the adverse effects of the drought from what we hypothesized were the adverse effects of the NO_2 pollution proved more difficult than anticipated. We planned to quantify water stress through a NDMI time series and quantify overall vegetation health through a NDVI time series. This is what we did, but not in the way that we first envisioned. The area containing CAVE and GUMO is classified as semi-arid, which yields sparse tree canopy. NDVI is a sufficient indicator of vegetation health in this environment, but NDMI is not as effective at indicating levels of water stress in vegetation that are found in semi-arid areas. We wanted to look at NDMI in the vegetation within CAVE and GUMO, but because NDMI uses the shortwave infrared band and the canopy coverage is sparse, a lot of the detected NDMI values were a result of moisture (or lack thereof) in the soil. We determined that this form of mapping water stress was still satisfactory because mapping a combination of water stress in vegetation and the soil is still objectively useful for assessing the effects of the drought.

We used Collection 2 Level 2 data for all Landsat imagery that was obtained. Level 2 data had much smaller NDVI values upon calculation than Level 1 did. This was determined to be inconsequential as we were going to be making change detection maps. Due to the nature of calculating a change detection map (Table B2)

there would be no difference if we used Level 2 or Level 1 data. Taking the percent difference between the two NDVI maps results in the same numbers regardless of using Level 1 or Level 2 data so long as the level is consistent throughout the data acquired. However, this did make the mean NDVI values observed lower for each of the study areas.

Out of the multiple ways to obtain Landsat images, we elected to use single scene Landsat images to assess vegetation health and water stress within the parks. The alternative option to this was to use Google Earth Engine and aggregate multiple Landsat images together to form a composite image of pixels that could have originated from various Landsat images. We elected to download single scenes for the purpose of continuity between pixels. In hindsight, the aggregation of images could have yielded cleaner and more representative data because it would have automatically averaged many NDVI and NDMI values over the course of the specific season rather than the values of just one day. If the single scene we use is an outlier, for example, and the image has a much higher NDVI due to the monsoon season arriving early, that whole scene is an outlier. Using aggregation methods, only some of the resulting image would be considered an outlier because it would not represent the entire image rather a percentage of it. Given how many confounding factors this project has, it could have been more beneficial to use an aggregation approach to Landsat imagery.

We also wanted to account for the confounding variable of wildfires as wildfires would impact NDVI and NDMI significantly on a year-to-year basis. Using the National Interagency Fire Center's (NIFC) Wildland Fire Locations Full History Dataset, we filtered our fire selection by fires that were within the study period, within the study area, and greater than 500 acres burned. The Coyote fire matched these criteria, discovered on 5/7/2016 and contained on 6/13/2016. Part of this fire occurred within GUMO (Figure C1). Luckily, the Landsat imagery we acquired for Spring 2016 was on 5/6/2016, which narrowly avoids the confounding effects for the wildfire in 2016. However, we did hypothesize that the effects of this wildfire could be seen in 2017 and beyond. This is likely the reason why the mean NDVI change from 2016-2017 in GUMO is –5.049 while the same change is +5.367 in CAVE and +0.095 in SDM respectively.

Another possible confounding variable that we accounted for was the impact of nitrogen deposition on vegetation. Nitrogen-containing air pollutants, such as NO_2, are the main drivers of nitrogen deposition across the world (Franz & Zaehle, 2021). As nitrogen is a limiting nutrient in terrestrial plant communities, nitrogen deposited onto vegetation by the NO_2 plume can stimulate photosynthetic activity and have a fertilization effect (Allen et al., 2010; Fenn, 2006). Fenn (2006) found that this effect could increase leaf and needle growth in pinyon and juniper, two of the most dominant vegetation types in the study area. We considered this when analyzing the results because such an increase in vegetation growth and productivity could offset some of the detrimental impacts O_3 has on vegetation, leading to unexpected increases in NDVI values (Franz & Zaehle, 2021). Thus, the growth stimulating effect of nitrogen deposition could explain the strongly inconsistent increase in NDVI (>25%) and decrease in NDMI (<50%) observed jointly in some parts of the study areas (Table 1, Figure 2).

4.2 Future Work

While we were unable to prove the hypothesis that the NO_2 plume is causing vegetation decline in CAVE and GUMO, the uncertainties and trends we encountered could be expanded on in future studies. For ease of acquisition and processing, our team relied on Landsat and IMERG data. However, different Earth observations could produce a variety of different indices to determine vegetation health. Sentinel-2's Multi-Spectral Instrument (MSI) carries three bands within the red-edge range, which would allow for analyzing chlorophyll indices such as the Inverted Red-Edge Chlorophyll Index (IRECI). This index is seen to have an almost 1:1 ratio with Leaf Area Index (LAI) in g/m^2, which can be reliably used in arid landscapes (Frampton et al., 2013). Moreover, the Enhanced Vegetation Index (EVI) is better suited for distinguishing lightly vegetated areas when compared to NDVI (Bhattarai, 2020). Regardless of sensor, many other vegetation indices could have been used. A Soil-Adjusted Vegetation Index (SAVI) or a Modified Soil-Adjusted Vegetation Index (MSAVI) requires a Red band, an NIR band, and additional adjustment factors (Qi et al.,

1994). These indices would contribute more accurate measurements to arid areas. Furthermore, there are multiple moisture indices suitable for this project.

We found grasslands and shrublands to be decreasing in CAVE and GUMO (Figure 2). However, it is likely that there would be more variation in the results using species-level aggregation. For instance, most of the Apacherian-Chihuahuan Semi-Desert Shrub-Steppe is in the eastern part of our CAVE study area, an area with substantial decrease in NDVI between 2010 and 2021 (Figure 2). The conifer class included more than pinyon and juniper species. Madrean Encinal dominated most of CAVE, but regularly co-occurs with pinyon and juniper (Texas Park and Wildlife, 2022). Future comparisons between NDVI and NDMI of different plant species could provide additional insight on the impacts of drought in the parks and find potential species-specific impacts of O_3 that we didn't find in this project. Changes in elevation also showed some correlation with both NDVI values and vegetation type. Higher elevations dominated by Pinyon-Juniper Woodland showed increases in NDVI, in contrast to decreases in NDVI found in shrubland-dominated lower elevations. Adding an elevational component to an analysis of NDVI and NDMI changes between plant species could yield more in-depth results on the ecosystems of CAVE and GUMO.

5. Conclusions

America's National Parks are a beacon of environmental progress designed to preserve areas of natural and historical significance. These areas protect a multitude of exotic species that cannot be found anywhere else in the world. For this reason, numerous forms of protection are put in place to prevent the deterioration of these parks. This includes efforts such as the Clean Air Act, which protects the parks from air pollution. Even with these protections, there are observed increases in NO_2 column densities in CAVE and GUMO. With this in mind, we analyzed data derived from Landsat 5 TM, Landsat 7 ETM+, Landsat 8 OLI, and IMERG to determine how the vegetation in the park responded to the NO_2 increase. We did not find conclusive evidence that NO_2 caused vegetation damage in CAVE and GUMO; although, we did find that vegetation health in the parks was increasing in some areas and decreasing in others. Vegetation in the higher elevations that mainly consisted of trees – such as pinyon and juniper – were experiencing an increase in NDVI despite the drought and increasing levels of NO_2, while vegetation in lower elevations consisting of mainly shrubland were experiencing a decrease in NDVI. This observed spatial distribution of NDVI as an indicator of vegetation health in the parks will aid partners in management decisions regarding the preservation of vegetation and ecosystem health within the parks. We also observed that there was an increase in water stress, in terms of NDMI, in all areas in the parks. This will help partners to increase their understanding of how the drought is affecting water availability in the area as well as water stress of the vegetation. We found that precipitation in CAVE and GUMO decreased over the study period. This means that partners can now confirm that there is a precipitation decrease in both parks, which will aid in quantifying water availability in the area. We illustrated these variations through maps created in ArcGIS Pro and graphs created in Microsoft Excel. Ecosystem health and vegetation health are vital to the maintenance of natural resources and the preservation of natural beauty and rarity of these National Parks. These products will equip partners with better insight and understanding to assist with park management policy.

6. Acknowledgments

The Delaware Basin Ecological Forecasting team would like to thank our partners from the NPS Intermountain Region for their collaboration and feedback on this project. We are also grateful to our science advisors, Joseph Spruce, Dr. Kenton Ross, and Dr. Elizabeth Wiggins, and to our fellow Adriana Le Compte, for their guidance, support, and technical assistance. The team would also like to thank the Delaware Basin Health & Air Quality Spring 2022 team for their invaluable contribution to this project.

DigitalGlobe/Maxar data were provided by NASA's Commercial Archive Data for NASA investigators (cad4nasa.gsfc.nasa.gov) under the National Geospatial-Intelligence Agency's NextView license agreement. Maps throughout this work were created using ArcGIS® software by Esri. ArcGIS® and ArcMap™ are the intellectual property of Esri and are used herein under license. All rights reserved.

Any opinions, findings, and conclusions or recommendations expressed in this material are those of the author(s) and do not necessarily reflect the views of the National Aeronautics and Space Administration.

This material is based upon work supported by NASA through contract NNL16AA05C.

7. Glossary

CAVE – Carlsbad Caverns National Park
Change Detection – Finding percent change in a value between two different temporal frames of reference
Delaware Basin – A structural basin in West Texas and Southern New Mexico that is part of the larger Permian Basin
Earth observations – Satellites and sensors that collect information about the Earth's physical, chemical, and biological systems over space and time
Fracking – A technique of injecting fluid into underground rock formations to open fissures that allow trapped gas or crude oil to flow through a pipe to the surface
GIF – Graphic Interchange Format
GDAL – Geospatial Data Acquisition Library
GPM – Global Precipitation Measurement
GUMO – Guadalupe Mountains National Park
IMERG – Integrated Multi-SatellitE Retrievals for GPM
LANDFIRE Vegetation Dataset – Dataset that utilizes Landsat imagery to find dominant vegetation type within a 30m x 30m area
Landsat 5 TM – Landsat 5 Thematic Mapper
Landsat 7 ETM+ – Landsat 7 Enhanced Thematic Mapper Plus
Landsat 8 OLI – Landsat 8 Operational Land Imagery
NDMI – Normalized Difference Moisture Index
NDVI – Normalized Difference Vegetation Index
NIR – Near Infrared
NO_2 – Nitrogen dioxide
NPS – National Park Service
Permian Basin – A large sedimentary basin in the Southwest United States known for its abundance in oil and natural gas
SDM – Sierra Diablo Mountains
SWIR – Shortwave Infrared
USGS – United States Geological Survey

8. References

Apurv, T., & Cai, X. (2021). Regional drought risk in the contiguous United States. *Geophysical Research Letters*, *48*(5). https://doi.org/10.1029/2020GL092200

Bhattarai, R. (2020). *Spruce Budworm Defoliation Detection and Host Species Mapping Using Sentinel Satellite Imagery*. [Master's thesis, The University of Maine]. DigitalCommons@UMaine. https://digitalcommons.library.umaine.edu/etd/3306/

The Census Bureau (2021). *Cartographic Boundary Shapefiles (*1:500,000) [Data set]. The Census Bureau. Cartographic Boundary Files (census.gov)

Cusick, S., Schlessiger, A., Henshaw, B., & Krisko, P. (2022) Delaware Basin Health & Air Quality: Spatiotemporal analysis of air pollutants collected from ground and space instruments around the Guadalupe Mountains and Carlsbad Caverns National Parks [Unpublished manuscript]. NASA DEVELOP National Program, Virginia – Langley.

Drilling Productivity Report. (2022). U.S. Energy Information Administration (EIA). https://www.eia.gov/petroleum/drilling/index.php

Frampton, W. J., Dash, J., Watmough, G., & Milton, E. J. (2013). Evaluating the capabilities of Sentinel-2 for quantitative estimation of biophysical variables in vegetation. *ISPRS Journal of Photogrammetry and Remote Sensing*, *82*, 83-92. https://doi.org/10.1016/j.isprsjprs.2013.04.007

Gabbert, Bill. (2016, May 10). *Strong wind causes Coyote Fire to awaken*. Wildfire Today. https://wildfiretoday.com/2016/05/10/coyote-fire-migrates-from-texas-into-new-mexico/

Gheorghe, I. F., & Ion, B. (2011). The effects of air pollutants on vegetation and the role of vegetation in reducing atmospheric pollution. *The Impact of Air Pollution on Health, Economy, Environment and Agricultural Sources*, *29*, 241-280. https://doi.org/10.1007/s13580-017-0053-0

Grulke, N. E., & Heath, R. L. (2020). Ozone effects on plants in natural ecosystems. *Plant Biology*, *22*, 12-37. https://doi.org/10.1111/plb.12971

Huffman, G. J., Stocker, E. F., Bolvin, D. T., Nelkin, E. J., Tan, J. (2019). *GPM IMERG Final Precipitation L3 1 month 0.1 degree x 0.1 degree V06*, Goddard Earth Sciences Data and Information Services Center (GES DISC). Retrieved July 5, 2022. https://doi.org/10.5067/GPM/IMERG/3B-MONTH/06

Jackson, R. B., Vengosh, A., Carey, J. W., Davies, R. J., Darrah, T. H., O'Sullivan, F., & Pétron, G. (2014). The environmental costs and benefits of fracking. *Annual Review of Environment and Resources*, *39*(1), 327-362. https://doi.org/10.1146/annurev-environ-031113-144051

Krupa, S. V., & Manning, W. J. (1988). Atmospheric ozone: Formation and effects on vegetation. *Environmental Pollution*, *50*(1-2), 101-137. https://doi.org/10.1016/0269-7491(88)90187-X

LANDFIRE (2022). *Landscape Fire and Resource Management Planning Tools* (Vegetation Type) [Data set]. U.S. Department of Agriculture Forest Service. LANDFIRE Program: Home

Landsat Missions (n.d.). *Landsat Normalized Difference Vegetation Index*. U.S. Geological Survey. https://www.usgs.gov/landsat-missions/landsat-normalized-difference-vegetation-index

Landsat Missions (n.d.). *Normalized Difference Moisture Index*. U.S. Geological Survey. https://www.usgs.gov/landsat-missions/normalized-difference-moisture-index

Markham, B. L., Storey, J. C., Williams, D. L., & Irons, J. R. (2004). Landsat sensor performance: history and current status. *IEEE Transactions on Geoscience and Remote Sensing, 42*(12), 2691-2694. https://doi.org/10.1109/TGRS.2004.840720

Meroni, M., Panigada, C., Rossini, M., Picchi, V., Cogliati, S., & Colombo, R. (2009). Using optical remote sensing techniques to track the development of ozone-induced stress. *Environmental Pollution*, *157*(5), 1413-1420. https://doi.org/10.1016/j.envpol.2008.09.018

National Park Service (2017). *Carlsbad Caverns National Park Tract and Boundary Data* (20170622) [Data set]. NPS – Land Resources Division. DataStore - Geospatial Dataset - (Code: 1047926) (nps.gov)

National Park Service (2018). *Geospatial data for the Vegetation Mapping Inventory Project of Guadalupe Mountains National Park* [Data set] NPS – Land Resource Division. DataStore - Geospatial Dataset - (Code: 2258337) (nps.gov)

Qi, J., Chehbouni, A., Huete, A. R., Kerr, Y. H., & Sorooshian, S. (1994). A modified soil adjusted vegetation index. *Remote Sensing of Environment*, *48*(2), 119-126. https://doi.org/10.1016/0034-4257(94)90134-1

Qu, C., Hao, X., & Qu, J.J. (2019). Monitoring extreme agricultural drought over the Horn of Africa (HOA) using remote sensing measurements. *Remote Sensing, 11*(8), 902. https://doi.org/10.3390/rs11080902

Roy, D. P., Kovalskyy, V., Zhang, H. K., Vermote, E. F., Yan, L., Kumar, S. S., & Egorov, A. (2016). Characterization of Landsat-7 to Landsat-8 reflective wavelength and normalized difference vegetation index continuity. *Remote Sensing of Environment*, *185*, 57-70. https://doi.org/10.1016/j.rse.2015.12.024

Sharifi, E., Steinacker, R.., & Saghafian, B. (2016). Assessment of GPM-IMERG and other precipitation products against gauge data under different topographic and climatic conditions in Iran: Preliminary results. *Remote Sensing*, *8*(2), 135. https://doi.org/10.3390/rs8020135

Texas Parks & Wildlife Department. (2022, January 26). *Madrean Encinal*. Madrean Encinal - Texas Parks & Wildlife Department. Retrieved July 28, 2022, from https://tpwd.texas.gov/landwater/land/programs/landscape-ecology/ems/emst/forests-woodlands-and-savannas/madrean-encinal

U.S. Geological Survey (2020). *Landsat 4-5 TM Collection 2 Level-2 Science Products*. [Data set]. USGS Earth Resources Observation and Science (EROS) Center. Retrieved June 22, 2022, from https://doi.org/10.5066/P9IAXOVV

U.S. Geological Survey (2020). *Landsat 7 ETM Plus Collection 2 Level-2 Science Products*. [Data set]. USGS Earth Resources Observation and Science (EROS) Center. Retrieved June 22, 2022, from https://doi.org/10.5066/P9C7I13B

U.S. Geological Survey (2020). *Landsat 8-9 OLI/TRIS Collection 2 Level-2 Science Products*. [Data set]. USGS Earth Resources Observation and Science (EROS) Center. Retrieved June 22, 2022, from https://doi.org/10.5066/P9OGBGM6

Vogelmann, J. E., Helder, D., Morfitt, R., Choate, M. J., Merchant, J. W., Bulley, H. (2001). Effects of Landsat 5 Thematic Mapper and Landsat 7 Enhanced Thematic Mapper plus radiometric and geometric calibrations and corrections on landscape characterization. *Remote Sensing of Environment*, *78*(1–2), 55-70. https://doi.org/10.1016/S0034-4257(01)00249-8

Xiong, H., Wu, W., & Gao, S. (2018, January 23). Optimizing well completion design and well spacing with integration of advanced multi-stage fracture modeling & reservoir simulation - a Permian Basin case study [Paper presentation]. SPE Hydraulic Fracturing Technology Conference and Exhibition, The Woodlands, Texas, USA. https://doi.org/10.2118/189855-MS

9. Appendices

Appendix A: Data Acquisition

Table A1

Data dictionary for datasets used for this project.

Parameter	**Source**	**Product Version / Level**	**Spatial Resolution**	**Temporal Resolution**	**Temporal Extent**
NDVI	Landsat 5 TM	Collection 2 Level 2	30m x 30m	Quarterly	January 2010 – January 2012
NDVI	Landsat 7 ETM+	Collection 2 Level 2	30m x 30m	Quarterly	January 2012 – April 2013
NDVI	Landsat 8 OLI	Collection 2 Level 2	30m x 30m	Quarterly	April 2013 – August 2021
NDMI	Landsat 5 TM	Collection 2 Level 2	30m x 30m	Quarterly	January 2010 – January 2012
NDMI	Landsat 7 ETM+	Collection 2 Level 2	30m x 30m	Quarterly	January 2012 – April 2013
NDMI	Landsat 8 OLI	Collection 2 Level 2	30m x 30m	Quarterly	April 2013 – August 2021
Precipitation	IMERG	Version 6 Level 3	0.1° x 0.1°	Monthly	January 2010 – August 2021

Appendix B: Data Processing and Analysis

Table B1

NDVI vs NDMI Regression Analysis

r^2	0.565		
Standard Error	0.017		
F-stat	118.168		**0.001**
	Coefficients	*T-stat*	
Intercept	0.176	40.035	**0.001**
NDMI	0.891	10.870	**0.001**

Table B2

Equations used for deriving indices and change detection

Index	**Equation**
Normalized Difference Vegetation Index (NDVI; Landsat Missions)	$\frac{NIR - RED}{NIR + RED}$
Normalized Difference Moisture Index (NDMI; Landsat Missions)	$\frac{SWIR - RED}{SWIR + RED}$
NDVI Conversion Factor (Roy et al., 2016)	$OLI = 0.9723(ETM+) + 0.0235$
NIR Conversion Factor (Roy et al., 2016)	$OLI = 0.8462(ETM+) + 0.0412$
SWIR Conversion Factor (Roy et al., 2016)	$OLI = 0.8937(ETM+) + 0.0254$
Percent Change	$\left(\frac{current - historic}{historic}\right) \cdot 100$

Appendix C: Coyote Fire Progression

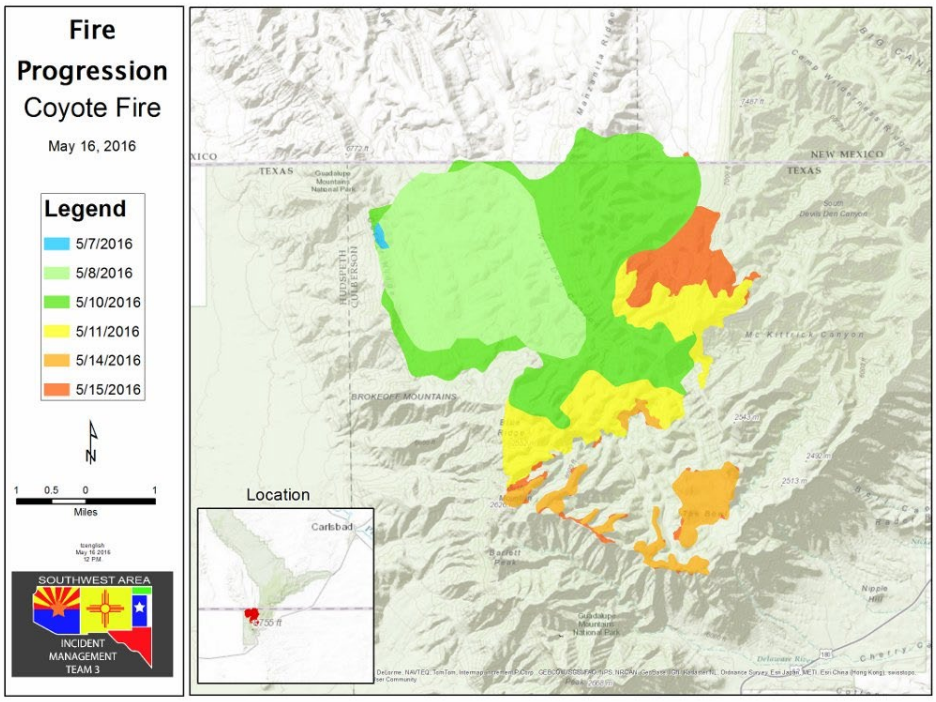

Figure C1. This map represents the progression of the Coyote Fire over time. Created by the NPS on May 16, 2016. Strong wind causes Coyote Fire to awaken. Wildfire Today. https://wildfiretoday.com/2016/05/10/coyote-fire-migrates-from-texas-into-new-mexico/

Appendix D: NO_2 Plumes

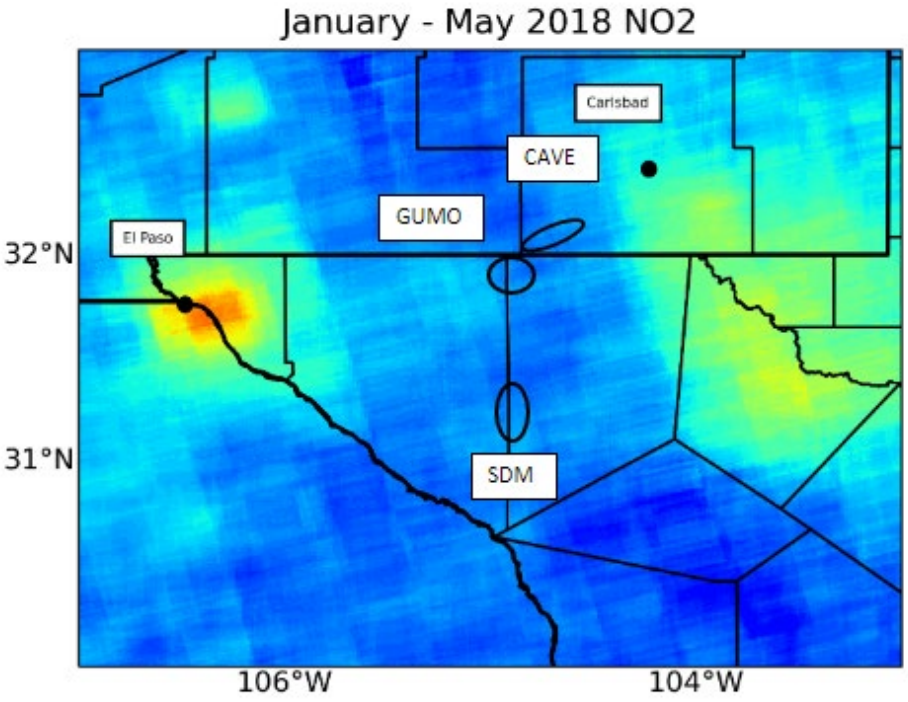

Figure D1. This map displays the location of NO_2 plumes over El Paso and the Delaware Basin (Cusick, Sean et al., 2022). Analysis of Air Pollutants from Ground and Space Instruments around Guadalupe Mountains and Carlsbad Caverns National Park [PowerPoint Slides].